Cholinergic modulation of hierarchical inhibitory control over cortical resting state dynamics: Local circuit modeling of schizophrenia-related hypofrontality

Marie Rooy [a,d,2], Ivan Lazarevich [a,e,2], Fani Koukouli [b,c,1], Uwe Maskos [b,c], Boris Gutkin [a,d,*]

[a] Ecole Normale Sup'erieure PSL Univeristy, Laboratoire de Neurosciences Cognitives INSERM U960, Group for Neural Theory, Paris, France
[b] Institut Pasteur, Neurobiologie integrative des systemes cholinergiques, Paris, France
[c] CNRS UMR 3571, Paris, France
[d] Center for Cognition and Decision Making, Institute of Cognitive Neuroscience, National Research University Higher School of Economics, Moscow, Russia
[e] Lobachevsky State University of Nizhny Novgorod, Nizhny Novgorod, Russia

ARTICLE INFO

ABSTRACT

Nicotinic acetylcholine receptors (nAChRs) modulate the cholinergic drive to a hierarchy of inhibitory neurons in the superficial layers of the PFC, critical to cognitive processes. It has been shown that genetic deletions of the various types of nAChRs impact the properties of ultra-slow transitions between high and low PFC activity states in mice during quiet wakefulness. The impact characteristics depend on specific interneuron populations expressing the manipulated receptor subtype. In addition, recent data indicate that a genetic mutation of the $\alpha 5$ nAChR subunit, located on vasoactive intestinal polypeptide (VIP) inhibitory neurons, the rs16969968 single nucleotide polymorphism ($\alpha 5$ SNP), plays a key role in the hypofrontality observed in schizophrenia patients carrying the SNP. Data also indicate that chronic nicotine application to $\alpha 5$ SNP mice relieves the hypofrontality. We developed a computational model to show that the activity patterns recorded in the genetically modified mice can be explained by changes in the dynamics of the local PFC circuit. Notably, our model shows that these altered PFC circuit dynamics are due to changes in the stability structure of the activity states. We identify how this stability structure is differentially modulated by cholinergic inputs to the parvalbumin (PV), somatostatin (SOM) or the VIP inhibitory populations. Our model uncovers that a change in amplitude, but not duration of the high activity states can account for the lowered pyramidal (PYR) population firing rates recorded in $\alpha 5$ SNP mice. We demonstrate how nicotine-induced desensitization and upregulation of the $\beta 2$ nAChRs located on SOM interneurons, as opposed to the activation of $\alpha 5$ nAChRs located on VIP interneurons, is sufficient to explain the nicotine-induced activity normalization in $\alpha 5$ SNP mice. The model further implies that subsequent nicotine withdrawal may exacerbate the hypofrontality over and beyond one caused by the SNP mutation.

1. Introduction

Alteration in the resting activity of the prefrontal cortex (PFC) occurs at the very onset of schizophrenia (Barch et al., 2001). Cortical acetylcholine (ACh) release exerts strong modulation of the PFC via the metabotropic muscarinic as well as the ionotropic nicotinic acetylcoline receptors. In this work, we focus on modelling the role of nicotinic acetylcholine receptors (nAChRs) in structuring the resting state PFC activity. These receptors are ligand-gated ion channels that mediate depolarizing current in response to ACh and nicotine. Within the layer II/III of the PFC nAChRs are specifically expressed on a hierarchically organized circuit of inhibitory neurons (Bloem et al., 2014). The subunit composition of these receptors determines their properties and their specific expression targets among the interneuronal populations. Individuals with nAChR gene variants appear to be susceptible to mental disorders and cognitive deficits (Sinkus et al., 2015; Koukouli and

Changeux, 2020). Notably, a mutation of the α5 nAChR subunit, the α5 SNP, has been observed in a subpopulation of patients with schizophrenia (Maskos, 2020). This mutation has been specifically linked to nicotine addiction and to a functional cortical deficit, hypofrontality, a characteristic of schizophrenia patients (Koukouli et al., 2017; Hong et al., 2010). Experiments in mice α5 SNP mutation show that the resting-state PFC neural activity exhibits a reduction that is qualitatively similar to the hypofrontality seen in humans. This tell-tale hypofrontality is reversed after 7 days of chronic nicotine application (Koukouli et al., 2017). In this work we build upon these findings and use computational modelling to support a specific hypothesis for the generative mechanism of the hypofrontality – that such hypofrontality is generated by a nicotinic receptor pathology in a local cortical circuit in the superficial layers of the PFC. More specifically, our model tests the hypothesis that the α5 SNP alters the hierarchical interneuronal inhibitory/disinhibitory layer II/III subcircuits within this local PFC circuit.

During quiet wakefulness, neural activity in layers II/III of the mouse PFC is characterized by synchronous ultra-slow fluctuations, with alternating periods of high and low activity (Koukouli et al., 2016a,b). Genetic knock-outs (KO) of specific nAChRs subunits were shown to disrupt these ultra-slow fluctuations, leading to changes in duration of high and low activity states (H-states and L-states, respectively). These patterns of activity are functionally significant since they may optimize information transmission in the context of lowered metabolism, such as quiet wakefulness, and because they could play an important role in

memory consolidation processes (Droste and Lindner, 2017). Furthermore, multi-stable dynamics in recurrent networks have been suggested to play a crucial role in working memory and decision-making processes (Durstewitz et al., 2000; Wong and Wang, 2006), as well as in disease (Koukouli et al., 2016a,b). Interestingly, patterns of hypofrontality in schizophrenia are associated with working memory deficits (Carter et al., 1998), hypothesized to be a core feature of the disease (Lee and Park, 2005).

Using the designed and validated local circuit computational model, we studied the modulatory role of the cholinergic inputs to the layer II/III GABAergic interneurons, mediated by the different nAChR subtypes. Specifically we focused on the nicotinic influence on the PFC ultra-slow fluctuations and the changes of the neural firing rate dynamics seen in mice with altered nAChR gene function. We used our model to examine the chronic nicotine impact on specific nAChR subunit-types to pinpoint the principal target of nicotine-dependent restoration of neural activity in α5 SNP mice. These modelling results may lend support to the self-medication hypothesis for smoking in schizophrenia patients as previously suggested in (Koukouli et al., 2017). Furthermore, we used our model to predict the consequence of nicotine withdrawal following chronic nicotine applications in α5 SNP mice. Our model showed a significant reduction in the PFC activity for this phenotype during nicotine withdrawal.

2. Methods

2.1. Neural population model

The model describes the dynamics of the firing rates of the various neuronal populations (r_e, r_p, r_s, and r_v, for PYR, PV, SOM and VIP neurons, respectively) in a local PFC circuit using a generalization of the Wilson-Cowan model (Papasavvas et al., 2015). We follow the theoretical framework for dominant subtractive vs. divisive inhibition by the SOM and PV interneuron populations, respectively (Chance and Abbott, 2000). Following (Chance and Abbott, 2000), we can heuristically justify this modelling choice, based on the relative location of the SOM and PV synapses on the layer II/III pyramidal neurons. SOM synapses are located largely on the distal part of the dendritic tree. They are electrotonically distant from the soma, hence their impact on the cell's activity is mostly subtractive (a de facto hyperpolarizing current). The PV interneurons tend to furnish synapses peri-somatically and onto the proximal dendritic segments, hence the synaptic conductance effects would yield a de facto divisive inhibition (synaptic-activation dependent reduction of the input resistance and change in the input-output pyramidal gain). See below for further discussion.

We further implemented structured subtractive inhibitory-inhibitory connections between SOM, VIP and PV interneuronal populations (Papasavvas et al., 2015). The full set of equations describing the firing rate dynamics of all the populations can be written as

$$
\begin{cases}
\tau_s \dfrac{dr_e}{dt} = -r_e + \left(A_e k_e\left(\omega_{pe} r_p\right) - r_e\right) F_e\left(\dfrac{\omega_{ee} r_e/A_e - (1 - k_d)\omega_{pe} r_p/A_p - \omega_{se} r_s/A_s + I_{ext-e}}{1 + k_d \omega_{pe} r_p/A_p}\right) + \sigma_s \xi(t). \\[4mm]
\tau_s \dfrac{dr_p}{dt} = -r_p + \left(A_p k_p - r_p\right) F_p\left(\dfrac{\omega_{ep} r_e}{A_e} - \dfrac{\omega_{pp} r_p}{A_p} - \dfrac{\omega_{vp} r_v}{A_v} + I_{ext-p}\right) + \sigma_s \xi(t) \\[4mm]
\tau_s \dfrac{dr_s}{dt} = -r_s + \left(A_s k_s - r_s\right) F_s\left(\dfrac{\omega_{es} r_e}{A_e} - \dfrac{\omega_{vs} r_v}{A_v} + I_{ext-s}\right) + \sigma_s \xi(t) \\[4mm]
\tau_s \dfrac{dr_v}{dt} = -r_v + \left(A_v k_v - r_v\right) F_v\left(\dfrac{\omega_{ev} r_e}{A_e} - \dfrac{\omega_{sv} r_s}{A_s} + I_{ext-v}\right) + \sigma_s \xi(t)
\end{cases}
\tag{1}
$$

with $I_{ext-p} = I_{0-p} + I_{\alpha7-p} + I_{adapt}$, $I_{ext-s} = I_{0-s} + I_{\alpha7-s} + I_{\beta2-s}$ and $I_{ext-v} = I_{0-v} + I_{\alpha5-v}$. $I_{\alpha7-p}$, $I_{\alpha7-s}$, $I_{\beta2-s}$ and $I_{\alpha5-v}$ are cholinergic external currents regulated by nAChRs. I_{0-p}, I_{0-s} and I_{0-v} are non-specific constant external currents. I_{adapt} is the adaptation current determined by equation (2) below.

We set $\tau_s = 20$ ms, close to each population type's membrane time constant (Pfeffer et al., 2013). F_x is a sigmoid response function characteristic of an excitatory (inhibitory) population, which gives a nonlinear relationship between input currents to a population, and its output firing rate. k_x modulate the amplitude of the firing rate response to an input current, dependent on PV activity for PYR neurons. See (Papasavvas et al., 2015) for the details of F_x and k_x functions, which are set by two constants, θ_x (minimum displacement) and α_x (maximum slope).

We note that most of the PV interneurons are Basket cells, and thus have a lower input resistance compared to PYR neurons (Beierlein et al., 2003). On the other hand, SOM interneurons, mostly Martinotti cells, and VIP interneurons have higher input resistance compared to PYR neurons (Beierlein et al., 2003). The highest input resistances are recorded in VIP interneurons (Beierlein et al., 2003). Hence, we changed the maximal slopes α_x according to those experimental findings (see table 1 in Supplementary Materials).

As mentioned above, we modelled PV modulation of PYR activity as a combination of both divisive and subtractive inhibition, which can be thought as more biologically realistic (Jadi et al., 2012; Wilson et al.,

2012). PV interneurons were specifically found to exert a divisive inhibition effect, which is assumed to be caused by powerful somatic, rather than dendritic, inhibition (Wilson et al., 2012). An additional constant parameter $k_d = 0.8$ is introduced in the model in order to express the fraction of divisive modulation that is delivered to the excitatory population. The rest of the modulation, $1 - k_d$, is delivered as subtractive.

The ω_{xx} (with $x \in \{e, p\}$) are the self-excitatory (or self-inhibitory) synaptic coupling weights of the excitatory (inhibitory) neural populations. The ω_{xy} (with $x \neq y$, $x \in \{e, p, s, v\}$ and $y \in \{e, p, s, v\}$) are the excitatory (or inhibitory) synaptic coupling weights from one population to another. We did not consider self-inhibition in the SOM and VIP interneuron populations, since inhibitory chemical synapses between those neurons are rarely observed (Pfeffer et al., 2013; Tremblay et al., 2016), and did not consider the direct SOM-PV connections in the main body of the paper, since regional discrepancies have been reported (Pfeffer et al., 2013; Gibson et al., 1999; Ma et al., 2012; Hu et al., 2011). However, we looked at the impact of these connections parametrically (see Fig. S11) and found that for a range of connectivity strengths our results were not significantly altered. The parameter σ_s controls the strength of fluctuations of neural populations' firing rate, and $\xi(t)$ is a Gaussian white noise with mean 0 and variance 1.

As in (Papasavvas et al., 2015), activities of the various neural populations were normalized in the range 0–0.5. We added factors (A_e, A_p, A_s, A_v) in order to fit the range of firing rates in the model to experimental values.

In order to model spike frequency adaptation in the PYR neuron population of the network model, we used the following equation, adapted from (Hayut et al., 2011):

$$\tau_{adapt}\frac{dI_{adapt}}{dt} = -I_{adapt} + r_e J_{adapt} \tag{2}$$

where τ_{adapt} and J_{adapt} are the adaptation time constant and the adaptation strength of the PYR population. We chose $\tau_{adapt} = 600$ ms according to (Destexhe, 2009). The resulting adaptation current I_{adapt} was added to the right hand side of the equation for the activity of the pyramodal population in eq. (1) above.

The modelling framework for the input terms dependent on the nicotinic acetylcholine receptors is described below.

2.2. Model parameter search procedure

The random search algorithm sampled 10^6 random parameter sets (points in parameter space), in a fixed value range for each parameter (values 1.0–55.0 for synaptic connection strengths, and 0.1 to 0.55 for external input currents). A single constraint was added to the parameter values of the model at this stage: VIP to PV connection strength value was set to be lower (by 50%) than VIP to SOM connection strength value (Hyun-Jae et al., 2013). After that, the parameter sets sampled by the random search algorithm were filtered out through a set of consecutive constraints:

● First, we performed a basic sanity check for each parameter set to determine if it could produce the bistable firing rate dynamics for the WT (baseline) parameter values. To do so, we computed the roots of the non-linear set of equations $dr_e/dt = 0$, $dr_p/dt = 0$, $dr_s/dt = 0$, $dr_v/dt = 0$, using MINPACK's hybrid and hybrj algorithms. We then selected the parameter sets that corresponded to the three roots of the above equations, hence two stable steady states of firing rate activity. These parameter sets represent $\sim 6\%$ of the total number of tested value sets.

● Second, we selected connection sets for which the normalized H-state is far from saturation (<0.45), and with a higher activity in H-state than L-state for all neuron types, so that the transitions between H-states and L-states are simultaneous across cell types. 93%, 61% and

96% of networks exhibited a higher PV, SOM and VIP activity all together in PYR high activity state (H-state) compared to the low activity state (L-state), according to experimental data.

● During the third step, parameters were selected based on residual error values for H- to L-state firing rate ratios for the simulated values versus the experimental ones. We fitted the scaling factors A_e, A_p, A_s, A_v so that the H-state for each simulated population type corresponded to the one found experimentally (to the median firing rate during the H-state in the experiments). We selected the networks for which the absolute error of the L-state rate level between the model and experiments did not exceed 5 spikes/min for each neural population type.

● From those selected networks, we simulated the firing rate time evolution of all neural types, in order to compute the distribution of H-state and L-state durations (with at least 500 state transitions in each simulation) for varying levels of noise σ_s (values between 0.001 and 0.02). For each given parameter set, we selected the noise level that best reproduced the mean and mode of H-state and L-state duration distributions in terms of the summed mean squared error. Then, for the matched noise level value, we selected parameter sets with low mean absolute percentage error (MAPE) values for the properties of ultraslow fluctuations extracted from the experimental data in WT animals (see table 2 in Supplementary Materials). Parameter sets corresponding to MAPE values below 100% were taken.

At this step of the parameter selection pipeline, we were left with $\sim$ 50 parameter set candidates out of the initially sampled 10^6 parameter sets. This "training" stage of the parameter selection procedure allowed us to effectively down select the large initial collection of models to several plausible ones using only the WT experimental data to formulate constraints.

In order to select one final of the 50 last parameter set candidates, we introduced an additional "validation" selection stage, which determined the model with the best predictive power outside the previously used WT data. Instead of pure WT data, for the validation stage we looked at the change of H-state firing rate levels between WT and $\alpha 5$ KO states. We chose the network in which the change of SOM H-state firing rate was the closest to the experimental value in terms of absolute error (see Supplementary Figs. S3E and S3F). Further on, we tested the selected parameter set against experimental data for all neural populations across different KO states. As we demonstrate, the selected model performs quite well during testing on KO states and predicts the key features of experimental data. Note that the other candidate parameter sets found during our search procedure also have relatively low values of the WT fitting error and decent performance when predicting activity levels in different knockout variants we considered (see Fig. S4). These parameter sets were selected based on the above procedure as leading to small values of the WT fitting error and well predicting the change in the SOM H-state firing rate in the $\alpha 5$ knockout state relative to the WT state. The set of candidate model parameters providing a good fit was found to span a relatively wide area in parameter space, however we found that all the major predictions inferred from the parameter set we ended up selecting were well reproduced qualitatively by the other found parameter sets. In particular, predictions concerning pyramidal population activity changes under nicotine treatment in wild-type and $\alpha 5$ SNP animals were found to be similar for different candidate parameter sets (see Fig. S4E).

2.3. Modeling nAChRs

We used a minimal model of subtype-specific activation and sensitization of nAChRs (Graupner et al., 2013), from which we determined the amplitude of each cholinergic current:

$$I_{x-n} = w_{x-n}a_x s_x, w_n = 0.01N_{x-n}, x \in \{\alpha 4\beta 2, \alpha 5\alpha 4\beta 2, \alpha 7\}, n \in \{s, p, v\} \tag{3}$$

where a_x is the activation variable, while s_x is the sensitization variable. They both take values between 0 and 1. The receptor is fully activated for $a_x = 1$ and fully sensitized for $s_x = 1$, while it is closed for $a_x = 1$ and fully desensitized for $s_x = 0$. We did not take into account desensitization of nAChRs by physiological levels of ACh because of its rapid breakdown through acetylcholinesterase (Graupner et al., 2013; Dani et al., 2001), such that $s_x = 1$. So the desensitization plays a role only for the nicotine simulations.

Using formulas from (Graupner et al., 2013), with $ACh = 1.77$ μM, relevant for in vivo simulations, we found $a_{\alpha4\beta2} = a_{\alpha5\alpha4\beta2} = 0.0487$, and $a_{\alpha7} = 0.0014$. N_{x-n} is the number of nAChRs of each type that best reproduced the changes of activity patterns recorded in experimental data (see Table 5 and Fig. 3A1-A2-A3). See Table 6 for the corresponding cholinergic currents. For the nicotine application simulations, we used a physiologically relevant blood concentration for smokers $Nic = 1$ μM

and computed the change in sensitization and activation of different nAChR types (see table 7). For $\alpha5\alpha4\beta2$ nAChRs, more resistant to desensitization, we shifted DC_{50} from 61 nM to 610 nM (Vladyslav and Harris, 2013). See table 8 for the corresponding cholinergic currents.

In the main body of the paper, we modelled the different KO mice by setting the corresponding cholinergic currents to zero. We also studied how the results depend on this assumption and found that the same trends in activity changes can be observed for small non-zero amplitudes of the nAChR currents, see Fig. 2. In particular, for the modelled $\alpha5$ SNP mice, expressing a human polymorphism of the $\alpha5$ nAChRs associated with both schizophrenia and heavy smoking, decreasing the VIP-expressed $\alpha5$ receptor activation by 30% was sufficient to give results compatible with the experiments.
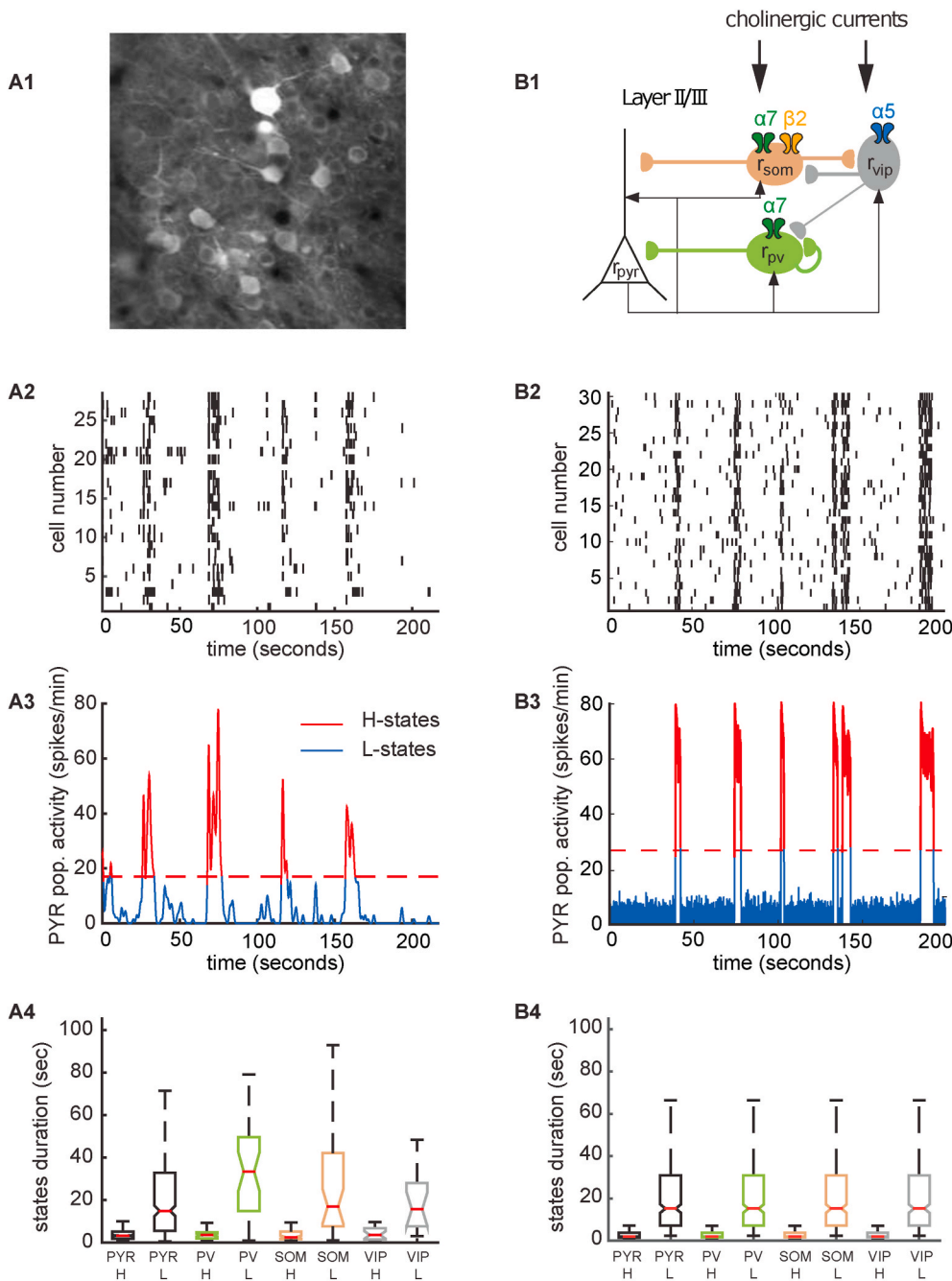
Fig. 1. Bistable firing rate dynamics of interconnected neural populations replicates ultra-slow fluctuations recorded in the PFC of WT mice. (A1) Two-photon image of GCaMP6f expressing neurons, from (Koukouli et al., 2017). (Scale bar: 20 μm). (A2) Inferred events of a population of simultaneously recorded cells in a WT mouse, obtained by deconvolving the spontaneous Ca2+ transients. 80% of the recorded cells are PYR neurons (Koukouli et al., 2017). (A3) Time varying population mean activity of the neurons shown in A2. The dashed red line delineates the threshold between high and low activity states (H-states and L-states, respectively). Red periods correspond to H-states and blue periods to L-states. See (Koukouli et al., 2016a,b) for more info on the methods. (A4) H-state and L-state durations recorded in the different neuron types. H-state durations are similar between neuron types (mean of 3 s, no statistical differences), as well as L-state durations (mean of 20 s, no statistical differences). (B1) Schematic of the studied circuitry. (B2) A simulated rastergram of neuronal activity, generated for illustration purposes from the population rate model, using a Poisson process with $\lambda(t) = mean\_population\_rate(t)$. (B3) Time varying mean population activity of pyramidal neurons, computed from the network model. We use the same method as (Koukouli et al., 2016a,b) to delineate H-states (in red) and L-states (in blue). (B4) The model reproduces the similar H-state and L-state durations across neural types. Distribution of a total of 500 state durations collected are plotted. (For interpretation of the references to colour in this figure legend, the reader is referred to the web version of this article.)

3. Results

3.1. Summary of the experimental approach and results

We studied experimentally the spontaneous activity of neurons in the prelimbic cortex of PFC in awake mice by two-photon calcium imaging (Koukouli et al., 2017). Male α7KO, β2KO, α5KO and WT C57BL/6J mice were used and experiments were performed at 3 months of age. Mice engineered to harbor the α5 D398N variant (α5SNP mice) were obtained via homologous recombination. Briefly, a chronic cranial window was prepared and 200 nl of AAV1.syn.GCaMP6f.WPRE.SV40 were injected bilaterally in the prelimbic cortex (PrL) (coordinates: AP, +2.8 mm from the bregma; L, $\pm$0.5 mm; DV, -0.3 to -0.1 mm from the skull) for recordings of pyramidal neurons. To record the activity of interneurons we used Cre mouse lines (VIP-Cre, SOM-Cre and PV-Cre

mouse lines) and 200 nl of AAV1.syn.Flex. GCaMP6f.WPRE.SV40 were injected as before. A sterile small stainless steel bar was embedded over the cerebellum in order to head-fix the mouse for imaging. Mice were trained for awake imaging by gentle handling for 4 days and were habituated to rest in a support tube on the mouse stage during the recordings, as previously described (Koukouli et al., 2017). *In vivo* imaging was performed using an Ultima IV two-photon laser-scanning microscope system (Bruker). For pyramidal neurons expressing GCaMP6f, time-series movies were acquired at the frame rate of almost 7 Hz, with a movie duration of approximately 215 s. The frame rate used for the interneuron recordings was about 30 Hz and the duration of each focal plane movie was approximately 165 s. Detection of individual neuron Ca^{2+} transients was performed automatically using a preprocessing and deconvolution pipeline written in MATLAB (Mathworks) (Koukouli et al., 2017).
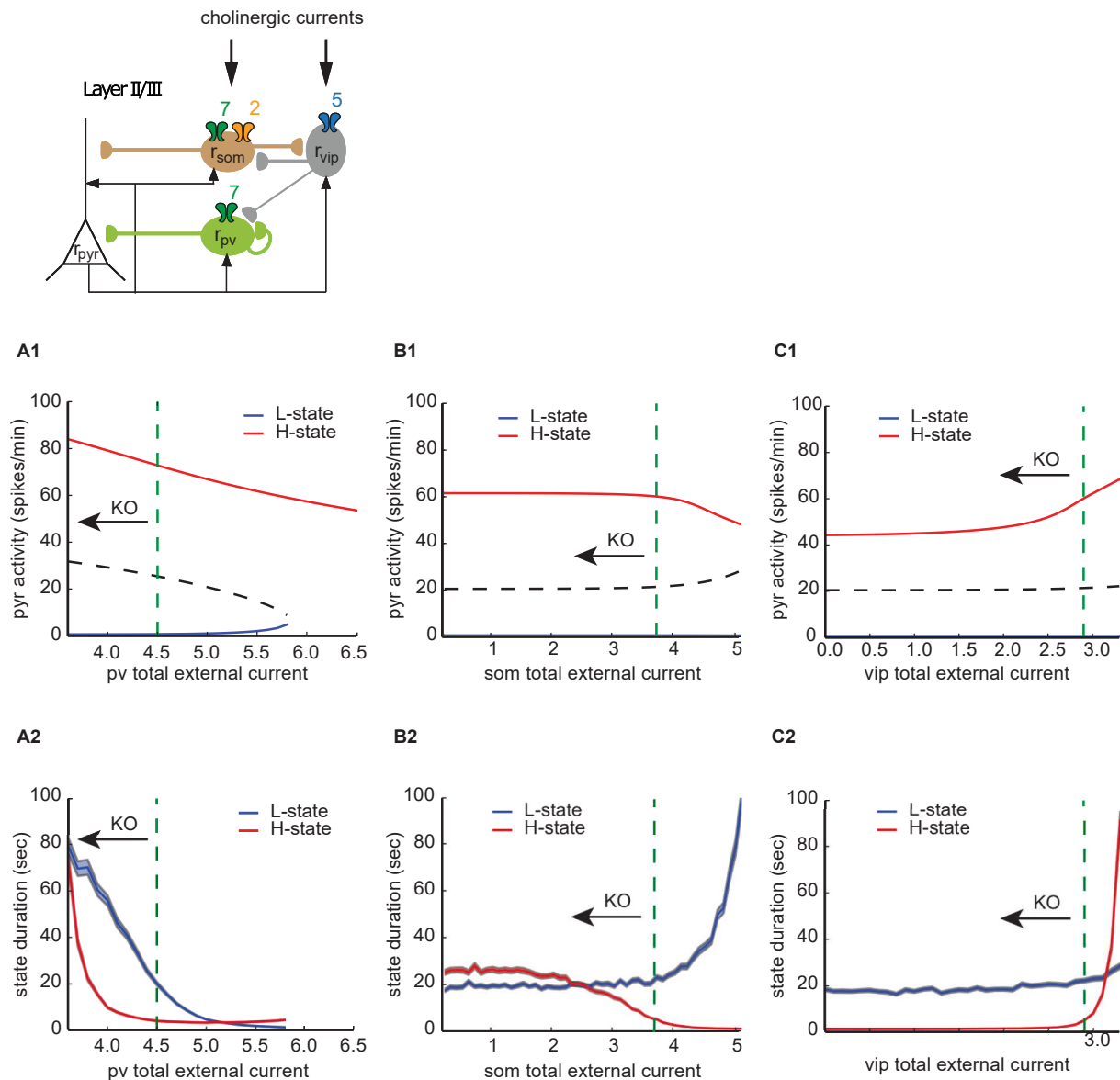
Fig. 2. Effects of changing external inputs to inhibitory populations on network state stability in the fully connected network (A1) H-state (red line) and L-state (blue line) PYR activities as a function of the external input current to VIP interneurons population. The dashed green line shows the selected parameter value to reproduce WT mice neural dynamics. KO of nAChRs is associated with a decrease of external currents (black arrow). (A2) H-state (red line) and L-state (blue line) durations as a function of the external input current to PV interneurons population. The shaded areas delineate $\pm$sem. The dashed green line shows the selected parameter value to reproduce WT mice neural dynamics. (B1) Same as (A1), but for the external input current to SOM INs population. (B2) Same as (A2), but for the external input current to SOM INs population. (C1) Same as (A1), but for the external input current to VIP INs population. (C2) Same as (A2), but for the external input current to VIP INs population. (For interpretation of the references to colour in this figure legend, the reader is referred to the web version of this article.)
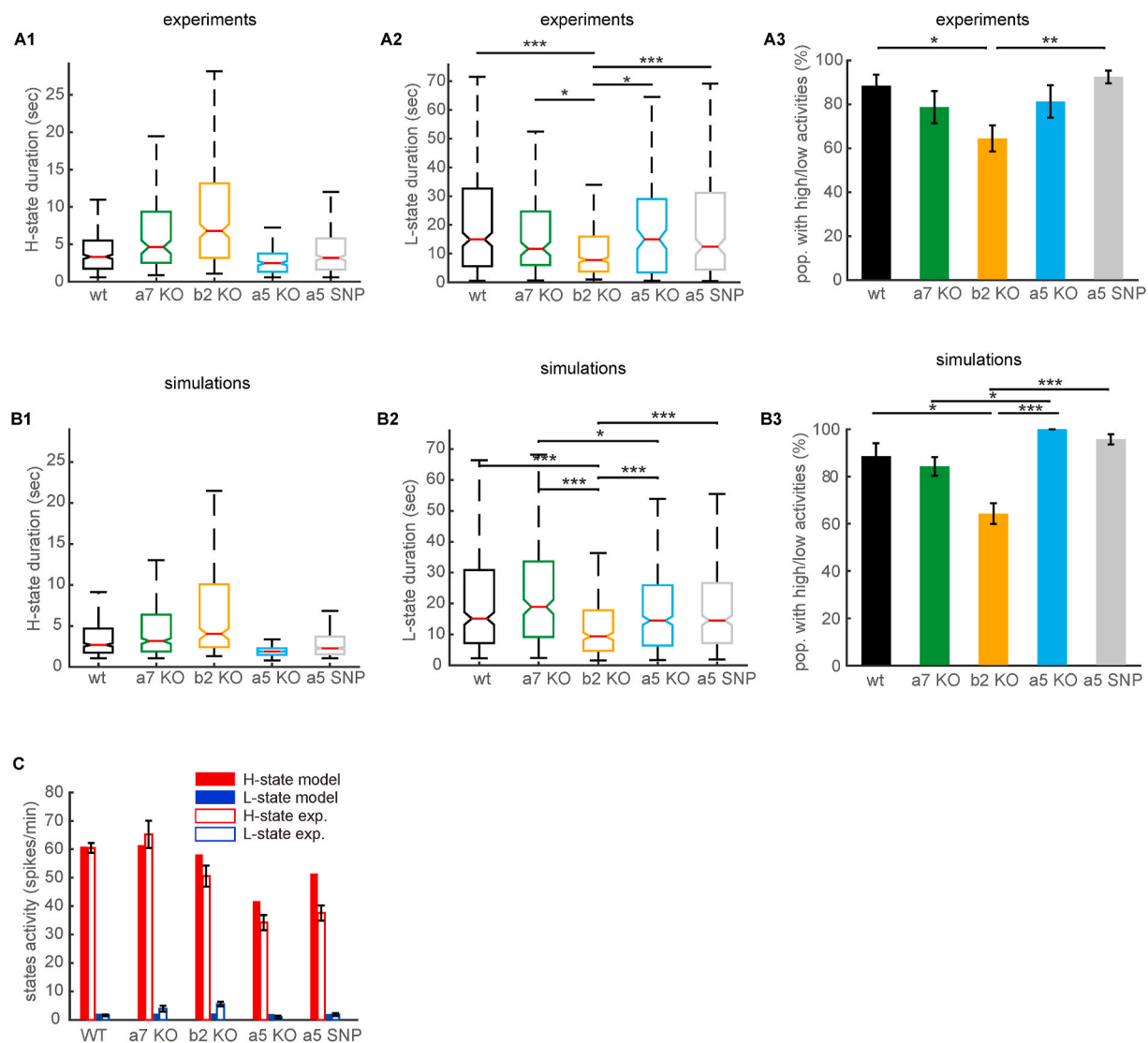
Fig. 3. Accounting for the nAChR KO and mutation impact on ultraslow fluctuations (A1) Mean of H-state durations, for WT and mutant mice, modified from Fig. 3C in (Koukouli et al., 2016a,b) for α7 KO and β2 KO mice. For α5 KO and α5 SNP mice, we use the same method as in (Koukouli et al., 2016a,b). All mutant mice distributions are significantly different from WT (Kruskal-Wallis, $P < 0.001$), except for α5SNP mice. The error bars are ±sem. (A2) Mean of L-state durations, for WT and mutant mice, modified from Fig. 3B in (Koukouli et al., 2016a,b) for α7 KO and β2 KO mice. β2 KO mice L-state durations are significantly lower compared to WT (Kruskal-Wallis, $P < 0.001$). The error bars are ±sem. (A3) Mean % of populations with H-states and L-states transitions. The error bars are ±sem. The circle shows the proportions computed for single mice. β2 KO mice exhibit significantly lower % of populations with H-states and L-states transitions (ANOVA, $P < 0.05$), compared to WT mice. Modified from Fig. 3D in (Koukouli et al., 2016a,b) for α7 KO and β2 KO mice. (B1-2-3) Same as (A1-2-3), computed from simulations. (C) H-states (red bars) and L-states (blue bars) activity levels from simulations (filled bars) and experiments (empty bars). Error bars are ±sem. Experimental data described in (Koukouli et al., 2016a,b). A total of 200 simulation repetitions with 500 state transitions each were carried out to produce the simulated data. (For interpretation of the references to colour in this figure legend, the reader is referred to the web version of this article.)

Briefly, we identified the temporal structure of the spontaneous activity in the layer II/III as alternating between low and high activity states (see Fig. 1A2-3 for an example of transition in a WT mouse). The typical time-scale of the high activity states (H-states) and low activity states (L-states) was on the order of several to tens of seconds. We then studied how the average activity and the temporal structure is altered by the experimentally induced genetic mutations of the nAChRs. Notably, we showed that mice expressing the human α5SNP exhibit reduced pyramidal cell activity. Our results also showed that the different nAChR subunits control the spontaneous PFC activity through a hierarchical inhibitory circuit. Specifically, in α5SNP mice and α5 KO mice, lower activity of VIP-expressing interneurons appeared to result in an increased SOM-interneuron inhibitory drive over the pyramidal neurons. Chronic nicotine administration reversed the hypofrontality observed in α5SNP mice through possible desensitization of β2-

containing nAChRs in SOM interneurons. Specific experimental data on the SNP as well as other KO mice will be shown below alongside the simulations for comparison and discussion of the circuit mechanisms.

3.2. Modelling formalism and strategy

For our local circuit model we used a neural population approach first pioneered by Wilson and Cowan (Destexhe and Sejnowski, 2009) and subsequently widely used in modelling studies. In this approach, the firing rates of cell ensembles are taken as the dynamical variables of the model (as opposed to modelling the biophysics of individual cells). Each variable in the model represents the activity of the specific cell-type population. The circuit is constructed by weighted connections between the cell populations so that the inputs to a given population represent the summarized synaptic connectivity between the neural

populations. External inputs to the circuit can be included in a similar way. These inputs are then put through a non-linear input-output function specific for each neuronal population.

Central to our work was to explicitly include the influence of the nicotinic cholinergic modulation exerted on specific cellular targets of the layer II/III PFC circuitry. We have previously shown how acetylcholine-dependent currents mediated by the nAChRs can be incorporated in the population rate models using simple kinetic schemes modified from (Katz and Thesleff, 1957) (see Methods and (Koukouli et al., 2017) for more details). The key point is that these currents can be parameterized to reflect the pharmacological and electrophysiological properties of specific receptor subtypes (temporal scales and ligand affinities for the activation and the desensitization) and incorporated into the specific neural population dynamics, reflecting their expression targets. We can then use the model to perform analysis, parameter fitting, validation and *in silico* genetic manipulation to understand how the local circuit dynamic mechanisms could explain the observed data. In other words, the strategy is to use a highly reduced model that distills away much biological complexity.

The logic for using such a highly reduced modelling approach is two-fold. First of all, the calcium imaging data analysis focused mainly on the dynamics and alterations of the mean activity of the recorded cell populations. Second, after incorporating the proposed structure of the local circuit and the relevant receptor-mediated currents, we were able to arrive at a model that was sufficient to explain key aspects of the data and yet was still tractable and understandable.

Overall, the circuit model was structured as shown in Fig. 1B. It reflects the hierarchical structure of the local inhibitory circuitry in the PFC layer II/III. Inspired by (Chance and Abbott, 2000) we used an extended Wilson-Cowan formalism to account for two kinds of inhibition impinging on the pyramidal neuron population: divisive inhibition due the PV interneurons and subtractive inhibition due to the SOM interneurons. Please note that the effect of PV interneurons was modelled as a mix of subtractive and divisive inhibition, reflecting that these neurons target the pyramidal cells peri-somatically and hence exert a shunting effect (Jadi et al., 2012). The ratio of divisive to subtractive inhibition in the model is controlled by the parameter k_d, Fig. S9 shows the robustness of the obtained results to the value of this parameter. The divisive inhibition acts to modulate the gain of PYR response, while the subtractive inhibition shifts this response. In fact one can heuristically think of two recurrent PYR-interneuronal pathways in this circuit: the PYR-PV divisive inhibitory one and the net additive disinhibitory one through the PYR-VIP-SOM neurons. We further included the inhibitory interactions between these sub-circuits. The specific neuronal population variables were also coupled to the nAChR models as indicated by the circuit scheme. As we will see below, the interplay of the recurrent excitation with the multiple interneuronal sub-circuits can lead to non-trivial dynamical outcomes in the model. The equations are described in full detail in the Methods.

Our strategy was to identify a model (i.e. the set of parameter values) that was able to account for the experimental data by first fitting the model parameters to match the control data of ongoing spontaneous activity, and then subjecting it to the simulated variations reflecting the genetic manipulations of the nAChRs. To do so we made an ansatz that the spontaneous high-low activity state alterations are due to a bistability in the local cortical circuit and the switching is controlled by random noise and firing rate adaptation in the PYR population. In order to identify the model regimes that could account for the experimental data, we used a multi-step model selection (fitting and validation) procedure (see Methods). First, we performed a semi-analytic analysis of the model dynamics as a function of the various inhibition strengths (see below). These results were then used as a guide for a global search procedure to identify a subset of model parameters that exhibited bistable dynamics. We then selected the model parameters so as to minimize the quantitative discrepancy (mean error) between the observed control experimental activity data and the data obtained by

simulating the model. We found that the connectivity parameters that minimize this error were generally widely distributed. We thus added further constraints on the model parameters. Since we were ultimately interested in accounting for the effects of the α5-SNP on the population firing patterns, we further selected the parameters so that we could focus on those models that could produce the mean activity changes when the ACh input to the VIP neurons was turned off. See Fig. S4 for the distribution of the fitting (control activity) and validation (knockout activity) errors across different parameters sets.

We then performed parametric manipulations of the receptor models to reflect the genetic alterations in the α7KO and β2KO animals (to validate the model on obtained experimental data), as well as to measure the influence of nicotine in those phenotypes. Below we present the model predictions for average firing activity level alterations in manipulated animals.

The details of model fitting and validation procedures are given in the Methods section; details of the calcium imaging analysis are given in (Koukouli et al., 2017). Further simulation results are given in the methods and the Supplement. Our model strategy and model selection procedures allowed us to potentially identify the local circuit pathways linking the genetic alterations and the in vivo PFC activity observations. Furthermore, we could use the model to profile future experiments and make predictions on the effects of nicotine withdrawal in the WT and α5SNP animal phenotypes.

Furthermore, we relaxed our model selection and examined multiple parametric sets of the model, to understand how the impact of the nicotinic receptor manipulations are distributed across multiple parameter sets (see Fig. S4). Indeed we found that there exist several different parameter sets that could predict the activity changes during simulated nAChR knockouts while giving a slightly worse fit in terms of the control wild-type data. Moreover, we found that the predictions regarding activity shifts during nicotine treatment were consistent across different parameter sets (see Fig. S4). Hence, the parameter set that we selected to obtain the main model predictions (marked as a red dot in Fig. S4) is representative of the whole model population.

3.3. Bistable layer II/III local PFC circuit firing rate dynamics replicate ultraslow fluctuations in WT mice

The basis for this modelling study are our experimental studies, briefly described above, of the spontaneous activity in the layers II/III of the prelimbic cortex in awake mice by two-photon calcium imaging (Koukouli et al., 2017). As shown by an example in Fig. 1A2-3, a population of simultaneously recorded cells in a WT mouse exhibits transitions between high activity states (H-states) and low activity states (L-states) lasting several to tens of seconds. We then set out to model the local circuitry that may produce this activity pattern. The circuit model sketched out in Fig. 1B1 simulates the firing rate evolution of populations of pyramidal (PYR) neurons intercoupled with a hierarchy of interneurons. Parvalbumin (PV) interneurons, expressing α7 nAChRs subunits (Bloem et al., 2014), target PYR cells axosomatically, with strong reciprocal connections (Holmgren et al., 2003). Somatostatin (SOM) interneurons, expressing both α7 and α4β2 nAChRs subunits (Bloem et al., 2014), target the dendrites of the PYR cells. The α5α4β2 nAChRs subunits are expressed only by vasoactive intestinal polypeptide (VIP) interneurons (Porter et al., 1999), that preferentially inhibit the SOM cells, and to a lesser extent PV cells (Hyun-Jae et al., 2013). Both the SOM and the VIP interneurons receive excitatory feedback from the PYR neurons (Silberberg and Markram, 2007; Porter et al., 1998). The model is able to reproduce the ultra-slow fluctuations of PYR population activity recorded in WT mice (Fig. 1B2-3) by assuming that two stable states of activity arise from the connectivity between neural populations (see Methods for more information on the model and fitting procedure). Simultaneous network transitions between activity states, for all neural types, drive the activity fluctuations. This prerequisite is consistent with our experimental findings, showing that the various neuron types have

similar H-state and L-state durations (Fig. 1A4 and B4 and Supplementary Fig. S6). Establishing that the local circuit model can replicate central properties of the WT data provided us with a computational model platform to turn to the data from the genetically modified animals.

3.4. Heuristic analysis of impact of inhibitory population activity variation on network state stability

Before proceeding to modelling the genetic nAChR manipulations, we wanted to develop an intuition about the influence of the different inhibitory inputs on the dynamics of the pyramidal neuron population using a reduced feed-forward inhibitory circuit (see Supplementary Materials). Here we explicitly differentiated the subtractive (SOM) versus the divisive (PV) inhibition. The PV-divisive inhibition controls the gain of the PYR input-output function. Our analysis showed that reducing the PV-divisive inhibition of the PYR population, increases this gain and makes both the high and the low states more stable. Therefore, decreases in the divisive inhibition should lead to increases in the state-durations during the spontaneous activity. Reducing the subtractive inhibition of the PYR population shifts the PYR activation function (without changing its shape). This leads to the low activity state becoming less stable and the high activity state gaining in stability. In other words, decreasing the SOM-dependent subtractive inhibition increases the duration of the H-states and decreases the duration of the L-states. Since the VIP neurons project to the SOMs and inhibit them, decreases in VIP activity lead to L-states increasing their durations and H-states becoming shorter on average. In summary, the preliminary analysis points out that SOM and VIP activity decrements should have an opposing effect on the PYR activity: former increasing it and latter decreasing it.

Taking the above into account, we now turn to the fully connected network, where we take into account the excitatory feedback from pyramidal neurons to the various interneurons subtypes, as well as the inhibitory inputs from VIP to PV neurons. We found that generally the simplified network intuition (see Supplementary Materials) holds for the full network (Fig. 2). The full model shows the expected increase of both H-state and L-state duration for decreased external inputs to PV population (Fig. 2B1). When the external inputs to the SOM population is decreased, we saw the predicted increase of H-state- and a decrease of L-state- duration for (Fig. 2B2). A decrease of H-state duration was seen for decreased external inputs to VIP population (Fig. 2C2). Note the shape of the bifurcation diagram as a function of the external input to PV population (Fig. 2A1). Due to the strong excitatory feedback from PYR to PV population (Lee and Park, 2005), for external inputs higher than a critical value, the network loses its bistability to a single H-state (as opposed to the single L-state in the simple version of the model, see Supplementary Fig. S1A3). Second, we observe a slight decrease of L-state duration for decreased external inputs to the VIP population (Fig. 2C2). This is where the VIP-PV connection plays the defining role: the decreased VIP activity increases the PV activity in both the H- and L-states (Fig. S7C1), which in turn decreases both H-state and L-state duration, due to the increased divisive inhibition impinging onto the PYR population. The results of this analysis indicate that if the knockout does not fully abolish the nAChR-mediated current, we would still observe the same qualitative behaviour in the modelled circuit, due to the smoothness and monotonicity of the activity level curves in Fig. 2. Interestingly, we observed the same trends in terms of increases/decreases of L- and H-state durations and firing rates for the different sets of parameters that we found during the model search procedure (the parameter set distribution is reflected in Fig. S4).

3.5. Impact of the nAChR genetic manipulations on the temporal structure of the ultraslow activity fluctuations

In order to analyze the nicotinic modulation of the resting state temporal structure through the β2-and α7-nAChR-mediated currents on their target inhibitory neurons, we explicitly modelled nAChR activation levels following a computational framework developed in (Graupner et al., 2013) (see also Methods). Our model reflected that the various receptor subclasses are expressed on specific neuronal targets (here exclusively on the different interneuronal subtypes). The model also took into account the ligand-gated electrophysiological properties of the modelled nAChR subclasses. According to the computational framework, β2 nAChRs, which have high affinity to acetylcholine (ACh), activate such that their cholinergically evoked input to the target cell population is ~35 fold the amplitude of the cholinergic current due to the α7 nAChRs. Note that due to the rapid ACh breakdown by the acetylcholinesterase (Dani et al., 2001; Giniatullin et al., 2005) and following our previously developed nAChR/neural circuit modelling framework, we chose not to take into account desensitization of nAChRs by physiological levels of ACh.

We then simulated our model with the *in silico* receptor knock-outs and tracked the duration of the high and low activity states as well as the proportion of neural populations (out of 100 simulated samples of our models generated from the pre-determined model parameter set as explained above) that showed the bistable dynamics. You can see in Fig. 3A1 that a knock-out of α7 nAChRs, located on both PV and SOM interneurons, induces an increase of H-state mean duration as compared to the WT animals, 4.2 ± 0.3 to 6.1 ± 0.5 s, with $P < 0.05$. Knock-outs of SOM-localized β2 nAChRs induce increased H-state durations (8.7 ± 0.5 s) that are much larger than those in the α7 KO animals. We modelled the KO case by setting the relevant receptor-mediated currents to zero. In our model we observed that setting the α7-mediated current to zero induces an increase of mean H-states duration from 4.0 ± 0.2 s, for simulated WT animals, to 5.6 ± 0.3 s, for simulated α7 KO animals ($P < 0.001$, see Fig. 3B1). The model also was able to account for the strong effect of the high affinity β2 nAChRs manipulation, with a more than 2-fold increase of H-state mean duration to 9.7 ± 0.8 s. The model further showed reduced H-state mean duration for the α5 KOs (2.0 ± 0.1, $P < 0.001$) compared to WT mice, similar to experimental findings (2.6 ± 0.2 s, $P < 0.001$). These results are consistent with α5-containing nAChRs having a modulatory effect on VIP activity, which in turn inhibit both PV and SOM interneurons. We found no significant changes in the H-state mean duration for α5 SNP compared to WT mice, both experimentally and through modeling (4.0 ± 0.3 s of H-state duration for experiments, and 3.3 ± 0.2 s for simulations). Our analysis above lead us to expect a significant decrease of mean L-state duration for β2 KO animals. Indeed we observed a drop from 22.6 ± 1.3 s to 13.9 ± 0.8 s, $P < 0.01$ (see Fig. 3B2), which we identify in the model as a combined effect of the decreased cholinergic input to the SOM and VIP populations, and which reproduces experimental findings (21.7 ± 1.3 s to 15.3 ± 1.0 s, $P < 0.001$, Fig. 3A2, modified from (Koukouli et al., 2017)). No significant change of L-state durations was found for α7, α5 and α5SNP compared to WT, both experimentally and through modeling. This is consistent with our prediction that VIP change of input to PV population, exerting divisive type of inhibition over PYR activity, would counterbalance VIP effects on L-state stability through SOM population (Fig. 2B3 and Fig. S1C3).

Having determined that our model can account for the mean statistics of the high-low spontaneous dynamics under various genetic manipulations of the nAChRs in the hierarchical inhibitory sub circuit of the PFC, we then examined the proportion of neural populations that would show bistable high-low dynamics in the spontaneous activity and how these are modified by the β2-receptor modulation. To do so, we constructed distribution histograms of the firing rates observed for a given phenotype (see also Methods and (Koukouli et al., 2017) for further analysis details) and identified what proportion of the populations showed multi-modal activity distributions. In our data (also see (Koukouli et al., 2017) for fuller discussion), we found that $65.9 \pm 5.7\%$ of populations exhibited high and low activity states transitions dynamics in β2 KO mice, a significant decrease compared to WT animals

(90.3 ± 5.0% of populations, $P < 0.05$, Fig. 3A3, modified from Koukouli et al., 2017) (Koukouli et al., 2017)). We simulated the $\beta2$ KO in our model by setting the cholinergic current strength terms to zero for the SOM neuron population. According to our model analysis, a decrease of cholinergic currents in the SOM population should induce an increase of H-state stability while a decrease of L-state stability (Fig. 2B2). Our simulations indeed reproduce the decreased proportion of populations exhibiting L-state/H-state transitions from 88.6 ± 3.6% in simulated WT animals to 64.3 ± 4.9% for simulated $\beta2$ KO mice (Fig. 3B3).

Furthermore, the model predicted that knocking out either the $\alpha7$ or the $\beta2$ nAChRs should decrease the H-state mean rate amplitude, and induce no changes in the L-state amplitudes, analysis of experimental data was in fact consistent with this prediction (see Fig. 3C).

3.6. Layer II/III circuit model accounts for the VIP and SOM neuron firing rate changes under schizophrenia-associated $\alpha5$ pathology

To further confirm our hypothesis that the decreased disinhibition in
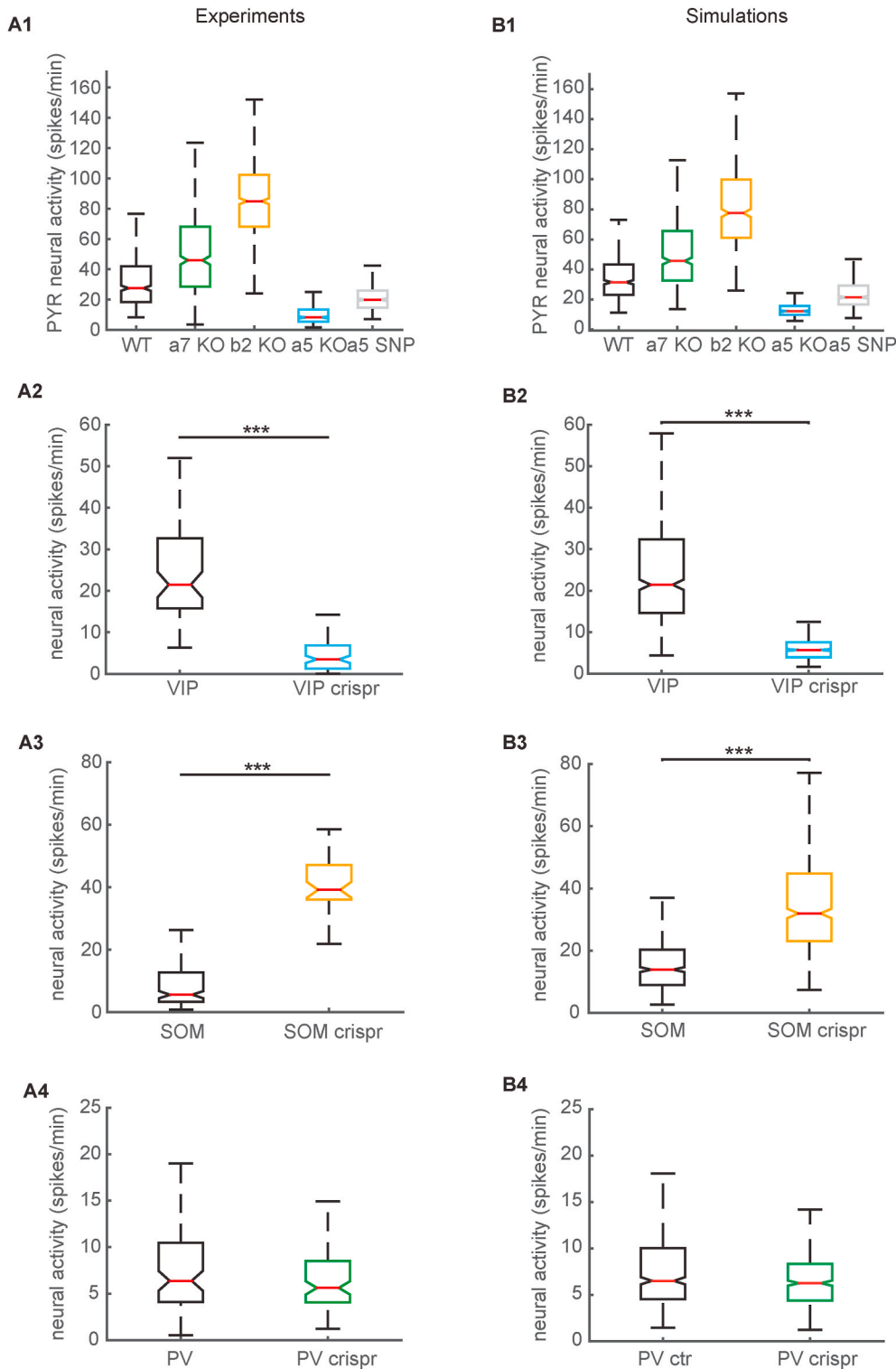
Fig. 4. Reproduction of the effects of KO and mutations of nAChRs on neural firing rates (A) Boxplots of PYR neurons firing rates for WT and mutant mice, computed from simulations. All distributions are significantly different (Kruskal-Wallis, $P < 0.001$). (B) Boxplots of VIP interneurons baseline activities for WT and CRISPR mice. CRIPSR mice exhibit lower neural activities compared to WT mice (Kruskal-Wallis, $P < 0.001$). (C) Boxplots of SOM interneurons baseline activities for WT and CRISPR simulated mice. CRIPSR mice exhibit higher neural activities compared to WT mice (Kruskal-Wallis, $P < 0.001$). (D) Boxplots of PV interneurons baseline activities for WT and mutant mice affected by the CRISPR technology for the deletion of the $\alpha5$ subunits, according to simulations. CRIPSR mice exhibit similar levels of neural activity compared to WT mice. A total of 200 simulation repetitions with 500 state transitions each were carried out to produce the simulated data.

α5 KO and α5 SNP mice accounts for hypofrontality, we compared the changes of VIP, PV, and SOM interneurons under α5 knock-down in experiments and simulations. In the experiments, clustered, regularly interspaced, short palindromic repeats (CRISPR)-associated endonuclease (Cas)9 technology was used to knock-down the α5 subunits in vivo, as shown in (Koukouli et al., 2017). We implemented this manipulation in the model by decreasing the activation of the a5-associated input to the VIP interneurons. Experimentally it was found that VIP neuron median activity decreased drastically under the CRISPR technology from 21.5 ± 2.17 spikes/min to 3.5 ± 0.7 spikes/min ($P <$ 0.001, see Fig. 3f in (Koukouli et al., 2017)). The model accounting for these results yielded decreased H-state network durations and decreased VIP H-state activity (see Fig. 3A1 and B1 and Supplementary Fig. S7C3). As a result, the simulated spike frequency of VIP interneurons in VIP α5 knock down mice (5.7 ± 0.2 spikes/min) was significantly lower than VIP neural activity in simulated WT animals (21.4 ± 1.2 spikes/min, $P <$ 0.001, see Fig. 4A2,B2). The model predicted that the decreased VIP levels of activity should result in increased levels of SOM activity through disinhibition. Experimental findings endorsed this prediction, through a robust increase in SOM interneuron spontaneous activity (39.1 ± 3.1 spikes/min) compared to control mice (5.6 ± 1.3 spikes/min, $P < 0.001$, see Fig. 3n in (Koukouli et al., 2017)). The model could reproduce this increase of SOM activity quantitatively (see Fig. Fig. 4C3) despite the significant decrease of network H-state duration (Fig. 3A1). Please note that the H-state durations are determined with all neuronal populations without being differentiated. In the model the over-all H-state duration decrease was associated with an unexpected increase in SOM H-state level of activity specifically (Supplementary Fig. S7C2). SOM WT mice simulated median activity increased from $13.9 \pm$ 0.7 spikes/min to 32.0 ± 1.2 spikes/min ($P < 0.001$, see Fig. 4C3). Experimentally, the decrease in PV interneuron activity was slight and not statistically significant (6.1 ± 0.6 spikes/min) compared to WT mice (5.6 ± 0.4 spikes/min, see Fig. 3j in (Koukouli et al., 2017)). We confirmed that in our model with parameters optimized to quantitatively reproduce the α5 SNP affect as reviewed above, we saw only a slight decrease of PV activity in CRSPR mice, as compared to WT simulated mice, from 7.9 ± 0.3 spikes/min to 5.0 ± 0.2 spikes/min ($P <$ 0.001). Because PV interneurons receive high levels of excitatory input from PYR neurons, we would expect a decrease of excitatory input to this population in α5 KO and CRISPR mice, due to decreased PYR neurons firing rate. This decreased excitatory input may be compensated by a decreased inhibition from the less active VIP interneurons, yet this connection is rather weak.

3.7. Nicotine re-normalizes α5 SNP PFC network activity through desensitization and upregulation of SOM β2 nAChRs

Experimentally it was observed that nicotine administration to α5 SNP mice by mini-pump infusion increased their PFC PYR neuron activity to WT levels (Koukouli et al., 2017), implying that it could reduce some of the cognitive deficits linked to schizophrenia, we used our model to pinpoint the specific nAChRs responsible for this normalization. We know that β2-dependent nAChR currents, but not α7, innervating interneurons in layer II/III of PFC, completely desensitize after exposure to smoking concentrations of nicotine in slice preparation (Poorthuis et al., 2013), with an exception for α5α4β2 nAChRs, that are more resistant to desensitization (Grady et al., 2012). Modeling nAChRs levels of activation and desensitization (Graupner et al., 2013) in contact of physiologically realistic levels of nicotine during smoking permits to predict the exact change of cholinergic currents amplitude, for each specific interneuron subtype. The model predicts activations of α7 and α5-containing nAChRs in contact of 1 μM of nicotine and a strong desensitization of β2-containing nAChRs (see table 6 and Fig. 5A1). As a result, you can see in Fig. 5A1 and A2 our predictions for PYR activity variations in WT and α5 SNP mice when nicotine targets selectively each type of nicotinic receptor. Desensitization of β2 nAChRs decreases

cholinergic inputs to SOM interneurons, and should increase the H-state network duration, leading to higher PYR firing rates in both WT and α5 SNP animals. An increase of cholinergic inputs to both SOM and PV interneurons, through the activation of α7 nAChRs, is assumed to induce a decrease of H-state durations, reducing PYR activity in WT and α5 SNP mice. Activation of α5 nAChRs, increasing cholinergic inputs to VIP interneurons, should disinhibit PYR neurons, causing higher PYR activities in both WT and α5 SNP mice. However, α5 SNP mice with α5 nAChRs activated by nicotine application still has lower PYR activities compared to WT mice without treatment.

According to our work, α5 nAChRs activation is not high enough to overcome α5 SNP receptor malfunction. As a consequence, in α5 SNP mice under treatment, higher PYR activities compared to WT control mice can only be replicated by nicotine interaction with β2 nAChRs located on SOM interneurons (Fig. 5A2). Experimental results (Fig. 4c in (Koukouli et al., 2017)) show that in both WT mice and α5 SNP mice, nicotine induces high increase of PYR activity after two days of nicotine administration, consistent with simulations predictions (see Fig. 5B). We know from our preliminary analysis in Fig. 5A2 and A3 that those effects are almost entirely due to the desensitization of β2 nAChRs on SOM interneurons.

We can notice in Fig. 4d, in (Koukouli et al., 2017), that the increase in PYR activity after 7 days of nicotine administration is reduced in both WT mice and α5 SNP mice compared to the 2 days treatment, such that PYR neurons firing rate in α5 SNP mice treated with nicotine are at the level of WT mice. Previous studies have indicated that long-term nicotine exposure over days increases or upregulates the number of high-affinity nicotine binding sites on α4β2 nAChRs (Govind et al., 2009). In addition to this, no nicotine-induced upregulation was observed for α5α4β2 nAChRs (Mao et al., 2008). Hence, we tested through modeling the effect of the upregulation of β2 nAChRs, located on SOM interneurons, on the PYR neuron firing rates. We were able to reproduce the normalization of PYR activity to WT levels in α5 SNP mice after 7 days of administration by considering a 1.8-fold increase of the number of β2 nAChRs located on SOM interneurons (see Fig. 5C). The factor by which one needs to increase the β2 nAChR current in the SOM population in order to reproduce this activity normalization was found to be similar for a range of different parameter sets found during model search (see Fig. S4), with a mean of about 1.7. You can see in Supplementary Fig. S8A1 that the increase of PYR activity in WT animals after 7 days of nicotine treatment is accompanied by an increase of H-state durations, that is reproduced in simulations (Fig. S8A2). It is also accompanied by a significant decrease of SOM activity (Fig. 4h in (Koukouli et al., 2017)), consistent with the model predictions (Fig. 5B).

Having validated our modelling framework on available experimental data, we set out to test the effects of nicotine withdrawal. We considered the neural circuit activity alterations that follow a 7-day nicotine application. We hypothesized that nicotine withdrawal would rapidly resensitize β2-containing nAChRs. On other hand, the renormalization of the number of receptors, which had been increased through upregulation, would occur on much slower time scales. As a result, the SOM interneurons would end up with higher levels of cholinergic innervation in the post-compared to the pre-treatment condition. Model simulations predict that WT and α5 SNP mice in the withdrawal condition to show a significant suppression of PYR activity as compared to the initial (pre-nicotine) state (Fig. 5D). Therefore our modelling results predict that post-nicotine withdrawal may exacerbate the α5 SNP-associated hypofrontality.

4. Discussion

In this work we developed a data-driven framework to model the influence exerted by nicotinic cholinergic neuromodulation of the hierarchical inhibitory local circuitry in the prefrontal cortex. We also showed how this inhibitory sub-circuit in turn controls the spontaneous resting state activity. We used the resulting computational model to
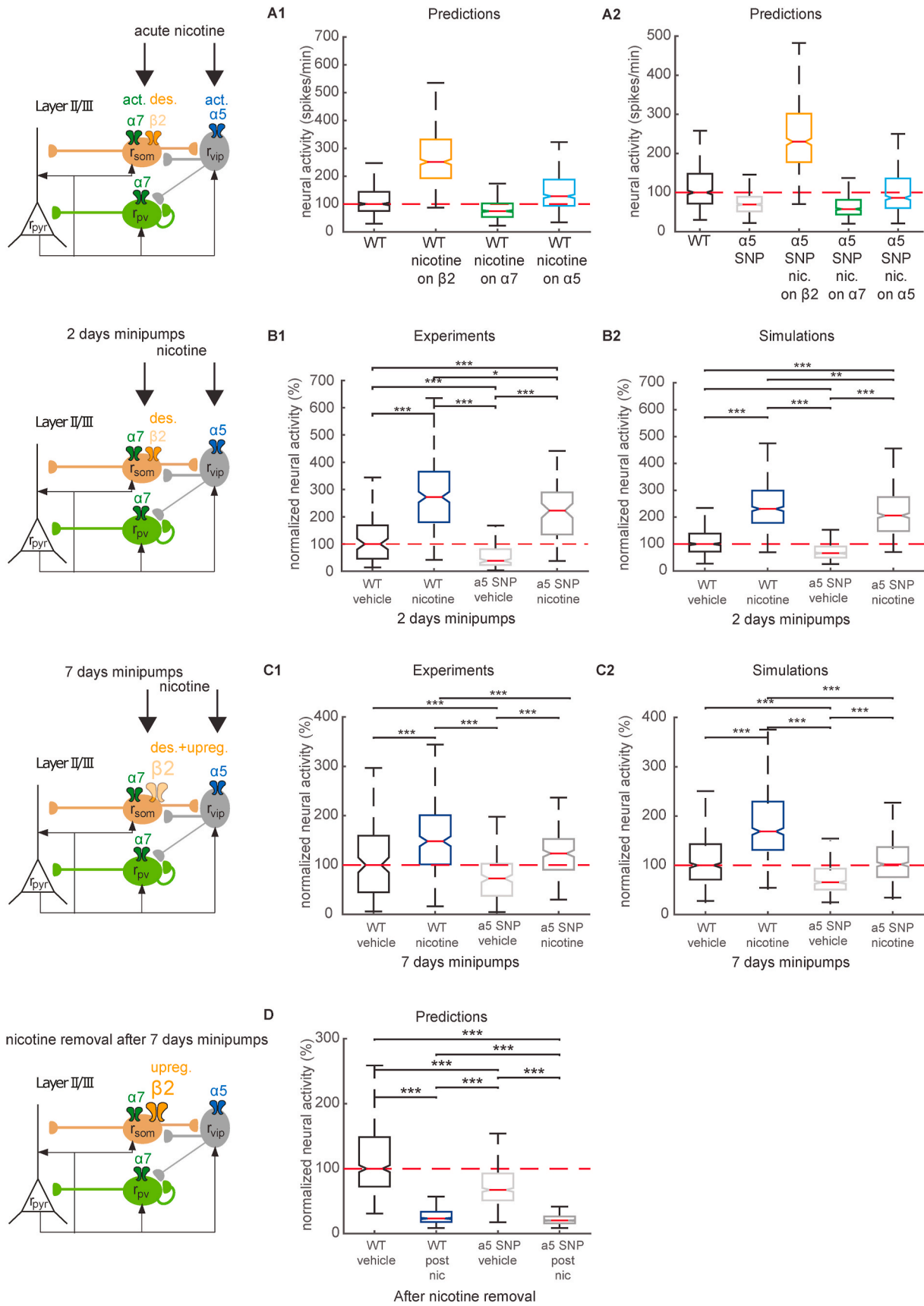
(caption on next page)

Fig. 5. Desensitization and upregulation of $\beta2$ nAChRs normalizes $\alpha5$ SNP mice network activity to WT levels after chronic nicotine application (A1) Distribution of PYR neurons firing rates for WT mice, computed from simulations of nicotine effects on $\alpha7$, $\beta2$, and $\alpha5$ nAChRs. All distributions are significantly different (Kruskal-Wallis, $P < 0.001$). (A2) Distribution of PYR neurons firing rates for WT and $\alpha5$SNP mice, computed from simulations of nicotine effects on $\alpha7$, $\beta2$, and $\alpha5$ nAChRs in $\alpha5$SNP mice. All distributions are significantly different (Kruskal-Wallis, $P < 0.001$). (B) Distribution of PYR neurons firing rates for WT and $\alpha5$SNP mice, control and treated with 2 days of chronic nicotine application, obtained from simulations. All distributions are significantly different (Kruskal-Wallis, $P < 0.001$). (C) Distribution of PYR neurons firing rates for WT and $\alpha5$SNP simulated mice, control and treated with 7 days of chronic nicotine application. All distributions are significantly different (Kruskal-Wallis, $P < 0.001$). The model predicts an upregulation of $\beta2$ nAChRs. (D) Distribution of PYR neurons firing rates for WT and $\alpha5$SNP mice, control and after nicotine removal following 7 days of chronic nicotine administration, predicted from simulations. All distributions are significantly different (Kruskal-Wallis, $P < 0.001$). A total of 200 simulation repetitions with 500 state transitions each were carried out to produce the simulated data.

account for effects of alterations in nAChR function by genetic manipulations and mutations associated with schizophrenia. We specifically applied to model to cellular imaging data obtained from the superficial layers of the prefrontal cortex of genetically modified mice in quiet wakefulness.

4.1. Summary of the results

What we learned from this modeling framework is two-fold.

First, the change of cholinergic input to the various GABAergic neurons, due to the knockout of various types of nAChRs, could fully account for the change of activity patterns recorded in the various mouse lines. The KO of the high-affinity $\beta2$ nAChRs, decreased the cholinergic input to the SOM population, thereby decreased the subtractive inhibition of PYRs. Decreasing this specific type of inhibition increases the stability of the network high activity states (H-states), increasing their durations. In addition reduction of SOM-mediated additive inhibition decreases the stability of the network low activity states (L-states), decreasing their durations. Simulated KO of $\alpha5$ nAChRs decreases the cholinergic inputs to the VIP interneuronal population, decreasing synaptic inhibition of SOM interneurons. This in turn increases the SOM-mediated inhibition of PYRs and leads to a significant decrease of H-state stability, decreasing their durations. However, this SOM-inhibition increase does not appear to lead to a significant increase of L-states durations. This is because the VIP inhibition of the PV neurons is also decreased, boosting the divisive inhibition of PYRs and having an opposite effect on L-state stability. Hence the impact of VIP alterations on the SOM-PYR inhibition and the PV-PYR inhibition balance out. The $\alpha7$ nAChR have a lower affinity to ACh. Hence KO of the $\alpha7$ nAChR leads to a relatively weaker decrease of cholinergic inputs to SOM and PV interneurons, which both, through subtractive and divisive inhibition respectively, increase the stability, thus durations, of the H-states.

Second, simulated 7-day nicotine application could restore the PYR activity to WT levels as compared to the $\alpha5$SNP case because of a mixture of desensitization and upregulation of $\beta2$ nAChRs. The model showed that activation of $\alpha5$ nAChRs by nicotine was not sufficient to compensate the $\alpha5$SNP activity deficits. Upregulation of $\beta2$ nAChRs after 7 days of treatment should lead to activity depression in both WT and $\alpha5$SNP cases when nicotine is removed, which could represent a highly critical situation in schizophrenia patients. Hence, this work provides experimentally testable predictions that the severity of symptoms in schizophrenia linked to decreased neural activity might increase upon nicotine withdrawal.

4.2. Predictions of the model

We summarize the predictions obtained with the proposed modelling framework as follows:

● Based on the constructed model, we hypothesize that the ultra-slow firing rate fluctuations in the prefrontal cortex are due to the internal bistable dynamics of the connected neuronal populations in the layer II/III PFC local circuit, with low-high activity state transitions triggered by inherent noise.
● The stability of the low-high states, and thus their life-times, are differentially controlled by a hierarchy of interneuronal populations.

In particular, PV interneurons are key in supporting the activity balance in the PFC circuit, with the synaptic VIP-PV connection pathway being dominant in controlling network bistability.
● Reduced pyramidal neuron activity in $\alpha5$ nAChR dysfunctions associated with schizophrenia (e.g. in $\alpha5$ SNP animals) can be normalized by enhancing the $\beta2$ nAChR activity, in particular under acute nicotine treatment.
● The model predicts that the existing $\alpha5$ SNP-associated hypofrontality can be significantly worsened by nicotine withdrawal.

4.3. Limitations of the model and future direction

The prefrontal cortex is a well-connected brain region receiving inputs from multiple brain regions. The complexity of the PFC circuitry, function and the multiplicity of the potential mechanisms that could influence its activity dynamics suggest that one may need to consider a range of compensatory, secondary and off-target effects when analysing experimental conditions like receptor knockout or/and nicotine treatment in animals (Bernard, 2020; Grashow et al., 2010; O'Leary et al., 2014; Wolff and Ölveczky, 2018). These multiple effects could be potentially reflected in the constructed computational models. However, in the scope of this work, we primarily focused on the cholinergic signaling components of the prefrontal cortex local circuitry as the main source triggering activity changes in the PFC. Within this reductionist approach to modelling, we were aiming to arrive at a minimal model that would be sufficient to explain our experimental data, assuming that the dynamics of the PFC circuitry is controlled by a hierarchy of interneurons expressing distinct nicotinic receptor types. While acknowledging that this is a strong hypothesis, there is experimental evidence supporting our local activity modulation proposal. Our previous experimental work (Koukouli et al., 2016a,b) demonstrated that targeted nicotinic acetylcholine receptor re-expression in layers II/III of the prelimbic cortex of the knockout mice completely restores pyramidal neuron activity to the levels of the wild-type mice, justifying our assumption that the activity change effects are due to receptor knockouts and are not significantly influenced by the developmental issues of the studied animals. This local re-expression also suggests that the effects we observed are unlikely to be simply due to changes in the inputs to our circuit. Furthermore, knockouts of $\beta2$-containing nAChRs were shown to completely shut down the activity of these receptors, with its complete restoration by local re-expression (Guillem et al., 2011; Maskos et al., 2005; Avale et al., 2008). Knockouts of $\alpha5$-containing nAChRs were found to cause dramatic shifts in dose-response curves for nicotine (Morel et al., 2014; Besson et al., 2018, 2019).

4.4. Implications for nicotine withdrawal in schizophrenia

Based on our work we may further speculate on the neurobiological explanation for the high prevalence of smoking and low smoking cessation rate observed among individuals with schizophrenia (Anthenelli et al., 2016). Our modelling framework gives predictions that nicotine cessation should decrease the prefrontal activity in both WT and the $\alpha5$SNP PFC, with the most drastic hypofrontality seen in $\alpha5$SNP mice under nicotine removal. This predicted exacerbated decrease of pyramidal activity is due to the upregulation of $\beta2$ nAChRs located on SOM interneurons, induced by several days of chronic nicotine

application. These model results beg the question: might not the lower cessation rates seen in schizophrenia patients be caused by a pronounced hypofrontality, induced by a combination of mutated $\alpha5$ nAChRs located on VIP interneurons and the upregulation of $\beta2$ nAChRs located on SOM interneurons. In fact, previous work showed that negative affect, one aspect of the negative schizophrenia symptoms associated with hypofrontality, is a key contributor to the low quitting rate seen in smoker schizophrenia patients (Jennifer et al., 2008). At the same time pharmacotherapy, through the use of varenicline, having similar nAChRs interaction mechanisms to nicotine, increases the abstinence rate in smokers and even more drastically in schizophrenia patient who are smokers (from 4.1% to 23.2%) (Anthenelli et al., 2016). We may suggest that these studies lend support to our hypothetical conjecture.

5. Conclusions

Schizophrenia is a severe mental disorder implicating a large variety of symptoms, among which apathy, abolition or social withdrawal, grouped as negative symptoms. Nowadays, no specific treatment can be recommended to treat negative aspects of schizophrenia pathology. Yet, it has been suggested recently that a mutation of a specific type of nicotinic receptor was implicated in the reduced neural activity levels recorded in the prefrontal cortex (PFC) of schizophrenia patients. Chronic nicotine injections in mice expressing this mutation ($\alpha5$ SNP mice) permits to restore neural activities to control levels, consistent with the idea that schizophrenia patients smoke to self-medicate. Using computational modeling, we showed that nicotinic receptors located on a hierarchy of inhibitory neurons were able to control ultra-slow neural activity fluctuations recorded in the PFC of mice. Furthermore, our modelling framework suggests that $\beta2$ receptors are the nicotine's main target in restoring neural activity to control levels in $\alpha5$ SNP mice. Lastly, we provide a testable model prediction that nicotine withdrawal in schizophrenia patients with the $\alpha5$ SNP mutation should lead to a progressively severe hypofrontality.

To cast a wider perspective to our circuit-based dynamic modelling approach opens a number of further avenues to both study specific disease-related alteration of nicotinic modulation in cortical circuits and to identify potential points-of-entry for therapeutic interventions.

CRediT authorship contribution statement

Marie Rooy: Conceptualization, Methodology, Software, Formal analysis, Investigation, Data curation, Writing – original draft. **Ivan Lazarevich:** Conceptualization, Methodology, Software, Formal analysis, Investigation, Data curation, Writing – original draft. **Fani Koukouli:** Conceptualization, Methodology, Investigation, Data curation, Writing – review & editing. **Uwe Maskos:** Conceptualization, Methodology, Writing – review & editing, Supervision. **Boris Gutkin:** Conceptualization, Methodology, Writing – original draft, Writing – review & editing, Supervision, Project administration, Funding acquisition.

Declaration of competing interest

The authors declare that they have no known competing financial interests or personal relationships that could have appeared to influence the work reported in this paper.

Acknowledgements

Appendix A. Peer Review Overview and Supplementary data

A Peer Review Overview and (sometimes) Supplementary data associated with this article can be found, in the online version, at https ://doi.org/10.1016/j.crneur.2021.100018.

References

Anthenelli, Robert M., Benowitz, Neal L., West, Robert, Aubin, Lisa St, McRae, Thomas, Lawrence, David, Ascher, John, Russ, Cristina, Krishen, Alok, Evins, A Eden, 2016. Neuropsychiatric safety and efficacy of varenicline, bupropion, and nicotine patch in smokers with and without psychiatric disorders (eagles): a double-blind, randomised, placebo-controlled clinical trial. Lancet 387, 2507–2520, 10037.

Avale, Maria Elena, Faure, Philippe, Pons, Stéphanie, Robledo, Patricia, Deltheil, Thierry and David, Denis, J., Gardier, Alain M., Maldonado, Rafael, Granon, 2008. Sylvie and Changeux, Jean-Pierre and others Interplay of $\beta2^*$ nicotinic receptors and dopamine pathways in the control of spontaneous locomotion. Proc. Natl. Acad. Sci. Unit. States Am. 105 (41), 15991–15996.

Barch, Deanna M., Carter, Cameron S., Braver, Todd S., Sabb, Fred W., MacDonald, Angus, Noll, Douglas C., Cohen, Jonathan D., 2001. Selective deficits in prefrontal cortex function in medication-naive patients with schizophrenia. Arch. Gen. Psychiatr. 58 (3), 280–288.

Beierlein, Michael, Gibson, Jay R., Connors, Barry W., 2003. Two dynamically distinct inhibitory networks in layer 4 of the neocortex. J. Neurophysiol. 90 (5), 2987–3000.

Besson, Morgane, Forget, Benoît, Correia, Caroline, Blanco, Rodolphe, Maskos, Uwe, 2018. A human polymorphism in CHRNA5 is linked to relapse to nicotine seeking in transgenic rats. Curr. Biol. 28 (20), 3244–3253.

Besson, Morgane, Forget, Benoît, Correia, Caroline, Blanco, Rodolphe, Uwe, Maskos, 2019. Profound alteration in reward processing due to a human polymorphism in CHRNA5: a role in alcohol dependence and feeding behavior. Neuropsychopharmacology 44 (11), 1906–1916.

Bloem, Bernard, Poorthuis, Rogier Bernard, Mansvelder, Huibert Daniel, 2014. Cholinergic modulation of the medial prefrontal cortex: the role of nicotinic receptors in attention and regulation of neuronal activity. Front. Neural Circ. 8 (17).

Carter, Cameron S., Perlstein, William, Ganguli, Rohan, Brar, Jaspreet, Mintun, Mark, Cohen, Jonathan D., 1998. Functional hypofrontality and working memory dysfunction in schizophrenia. Am. J. Psychiatr. 155 (9), 1285–1287.

Chance, Frances S., Abbott, L.F., 2000. Divisive inhibition in recurrent networks. Netw. Comput. Neural Syst. 11 (2), 119–129.

Bernard, Christophe, 2020. On Fallacies in neuroscience. Eneuro 7, 6.

Dani, John A., Ji, Daoyun, Zhou, Fu-Ming, 2001. Synaptic plasticity and nicotine addiction. Neuron 31 (3), 349–352.

Destexhe, Alain, 2009. Self-sustained asynchronous irregular states and up–down states in thalamic, cortical and thalamocortical networks of nonlinear integrate-and-fire neurons. J. Comput. Neurosci. 27 (3), 493.

Destexhe, Alain, Sejnowski, Terrence J., 2009. The wilson–cowan model, 36 years later. Biol. Cybern. 101 (1), 1–2.

Droste, Felix, Lindner, Benjamin, 2017. Up-down-like background spiking can enhance neural information transmission. Eneuro 4 (6).

Durstewitz, Daniel, Seamans, Jeremy K., Sejnowski, Terrence J., 2000. Neurocomputational models of working memory. Nat. Neurosci. 3 (11), 1184–1191.

Gibson, Jay R., Beierlein, Michael, Connors, Barry W., 1999. Two networks of electrically coupled inhibitory neurons in neocortex. Nature 402 (6757), 75–79.

Silberberg, Gilad, Markram, Henry, 2007. Disynaptic inhibition between neocortical pyramidal cells mediated by martinotti cells. Neuron 53 (5), 735–746.

Giniatullin, Rashid, Nistri, Andrea, Yakel, Jerrel L., 2005. Desensitization of nicotinic ach receptors: shaping cholinergic signaling. Trends Neurosci. 28 (7), 371–378.

Govind, Anitha P., Paul, Vezina, Green, William N., 2009. Nicotine-induced upregulation of nicotinic receptors: underlying mechanisms and relevance to nicotine addiction. Biochem. Pharmacol. 78 (7), 756–765.

Grady, Sharon R., Wageman, Charles R., Patzlaff, Natalie E., Marks, Michael J., 2012. Low concentrations of nicotine differentially desensitize nicotinic acetylcholine receptors that include $\alpha5$ or $\alpha6$ subunits and that mediate synaptosomal neurotransmitter release. Neuropharmacology 62 (5–6), 1935–1943.

Grashow, Rachel, Brookings, Ted, Marder, Eve, 2010. Compensation for variable intrinsic neuronal excitability by circuit-synaptic interactions. J. Neurosci. 30 (27), 9145–9156.

Graupner, Michael, Maex, Reinoud, Gutkin, Boris, 2013. Endogenous cholinergic inputs and local circuit mechanisms govern the phasic mesolimbic dopamine response to nicotine. PLoS Comput. Biol. 9 (8), e1003183.

Guillem, Karine, Bloem, Bernard, Poorthuis, Rogier B., Loos, Maarten, Smit, August B., Maskos, Uwe, Spijker, Sabine, Mansvelder, Huibert D., 2011. Nicotinic acetylcholine receptor $\beta2$ subunits in the medial prefrontal cortex control attention. Science 333 (6044), 888–891.

Hayut, Itai, Fanselow, Erika E., Connors, Barry W., Golomb, David, 2011. Lts and fs inhibitory interneurons, short-term synaptic plasticity, and cortical circuit dynamics. PLoS Comput. Biol. 7 (10), e1002248.

Holmgren, Carl, Harkany, Tibor, Svennenfors, Björn, Zilberter, Yuri, 2003. Pyramidal cell communication within local networks in layer 2/3 of rat neocortex. J. Physiol. 551 (1), 139–153.

Hong, L Elliot, Hodgkinson, Colin A., Yang, Yihong, Sampath, Hemalatha, Ross, Thomas J., Buchholz, Brittany, Salmeron, Betty Jo, Srivastava, Vibhuti, Thaker, Gunvant K., Goldman, David, et al., 2010. A genetically modulated, intrinsic cingulate circuit supports human nicotine addiction. Proc. Natl. Acad. Sci. Unit. States Am. 107 (30), 13509–13514.

Hu, Hang, Ma, Yunyong, Agmon, Ariel, 2011. Submillisecond firing synchrony between different subtypes of cortical interneurons connected chemically but not electrically. J. Neurosci. 31 (9), 3351–3361.

Hyun-Jae, Pi, Hangya, Balázs, Duda, Kvitsiani, Sanders, Joshua I., Huang, Z Josh, Adam, Kepecs, 2013. Cortical interneurons that specialize in disinhibitory control. Nature 503 (7477), 521–524.

Jadi, Monika, Alon, Polsky, Schiller, Jackie, Bartlett, W Mel, 2012. Location-dependent effects of inhibition on local spiking in pyramidal neuron dendrites. PLoS Comput. Biol. 8 (6), e1002550.

Jennifer, W Tidey, Damaris, J Rohsenow, Kaplan, Gary B., Swift, Robert M., Amy, B Adolfo, 2008. Effects of smoking abstinence, smoking cues and nicotine replacement in smokers with schizophrenia and controls. Nicotine Tob. Res. 10 (6), 1047–1056.

Katz, Bernard, Thesleff, S., 1957. A study of the desensitization'produced by acetylcholine at the motor end-plate. J. Physiol. 138 (1), 63.

Koukouli, Fani, Rooy, Marie, Maskos, Uwe, 2016a. Early and progressive deficit of neuronal activity patterns in a model of local amyloid pathology in mouse prefrontal cortex. Aging (Albany NY) 8 (12), 3430.

Koukouli, Fani, Rooy, Marie, Changeux, Jean-Pierre, Maskos, Uwe, 2016b. Nicotinic receptors in mouse prefrontal cortex modulate ultraslow fluctuations related to conscious processing. Proc. Natl. Acad. Sci. Unit. States Am. 113 (51), 14823–14828.

Koukouli, Fani, Changeux, Jean-Pierre, 2020. Do nicotinic receptors modulate high-order cognitive processing? Trends Neurosci. 43, 550–564.

Koukouli, Fani, Rooy, Marie, Tziotis, Dimitrios, Sailor, Kurt A., O'Neill, Heidi C., Levenga, Josien, Witte, Mirko, Nilges, Michael, Changeux, Jean-Pierre, Hoeffer, Charles A., et al., 2017. Nicotine reverses hypofrontality in animal models of addiction and schizophrenia. Nat. Med. 23 (3), 347–354.

Lee, Junghee, Park, Sohee, 2005. Working memory impairments in schizophrenia: a meta-analysis. J. Abnorm. Psychol. 114 (4), 599.

Ma, Yunyong, Hu, Hang, Agmon, Ariel, 2012. Short-term plasticity of unitary inhibitory-to-inhibitory synapses depends on the presynaptic interneuron subtype. J. Neurosci. 32 (3), 983–988.

Mao, Danyan, Perry, David C., Yasuda, Robert P., Wolfe, Barry B., Kellar, Kenneth J., 2008. The $\alpha 4 \beta 2 \alpha 5$ nicotinic cholinergic receptor in rat brain is resistant to up-regulation by nicotine in vivo. J. Neurochem. 104 (2), 446–456.

Maskos, Uwe, 2020. The nicotinic receptor alpha5 coding polymorphism rs16969968 as a major target in disease: functional dissection and remaining challenges. J. Neurochem. (154), 241–250. https://doi.org/10.1111/jnc.14989.

Maskos, Uwe, Molles, B.E., Pons, S., Besson, M., Guiard, B.P., Guilloux, J.-P., Evrard, A., Cazala, P., Cormier, A., Mameli-Engvall, M., et al., 2005. Nicotine reinforcement and cognition restored by targeted expression of nicotinic receptors. Nature 436 (7047), 103–107.

Morel, C., Fattore, L., Pons, Stéphanie, Hay, Y.A., Marti, F., Lambolez, B., De Biasi, M., Lathrop, M., Fratta, Walter, Maskos, Uwe, et al., 2014. Nicotine consumption is regulated by a human polymorphism in dopamine neurons. Mol. Psychiatr. 19 (8), 930–936.

O'Leary, Timothy, Williams, Alex H., Franci, Alessio, Marder, Eve, 2014. Cell types, network homeostasis, and pathological compensation from a biologically plausible ion channel expression model. Neuron 82 (4), 809–821.

Papasavvas, Christoforos A., Wang, Yujiang, Trevelyan, Andrew J., Kaiser, Marcus, 2015. Gain control through divisive inhibition prevents abrupt transition to chaos in a neural mass model. Phys. Rev. 92 (3), 032723.

Pfeffer, Carsten K., Xue, Mingshan, He, Miao, Huang, Z Josh, Scanziani, Massimo, 2013. Inhibition of inhibition in visual cortex: the logic of connections between molecularly distinct interneurons. Nat. Neurosci. 16 (8), 1068–1076.

Poorthuis, Rogier B., Bloem, Bernard, Schak, Benita, Wester, Jordi, de Kock, Christiaan PJ., Huibert, D Mansvelder, 2013. Layer-specific modulation of the prefrontal cortex by nicotinic acetylcholine receptors. Cerebr. Cortex 23 (1), 148–161.

Porter, James T., Bruno, Cauli, Staiger, Jochen F., Lambolez, Bertrand, Rossier, Jean, Audinat, Etienne, 1998. Properties of bipolar vipergic interneurons and their excitation by pyramidal neurons in the rat neocortex. Eur. J. Neurosci. 10 (12), 3617–3628.

Porter, James T., Bruno, Cauli, Tsuzuki, Keisuke, Lambolez, Bertrand, Rossier, Jean, Audinat, Etienne, 1999. Selective excitation of subtypes of neocortical interneurons by nicotinic receptors. J. Neurosci. 19 (13), 5228–5235.

Sinkus, Melissa L., Graw, Sharon, Freedman, Robert, Ross, Randal G., Lester, Henry A., Leonard, Sherry, 2015. The human chrna7 and chrfam7a genes: a review of the genetics, regulation, and function. Neuropharmacology 96, 274–288.

Tremblay, Robin, Lee, Soohyun, Rudy, Bernardo, 2016. Gabaergic interneurons in the neocortex: from cellular properties to circuits. Neuron 91 (2), 260–292.

Vladyslav, V Vyazovskiy, Harris, Kenneth D., 2013. Sleep and the single neuron: the role of global slow oscillations in individual cell rest. Nat. Rev. Neurosci. 14 (6), 443–451.

Wilson, Nathan R., Runyan, Caroline A., Wang, Forea L., Sur, Mriganka, 2012. Division and subtraction by distinct cortical inhibitory networks in vivo. Nature 488 (7411), 343–348.

Wolff, Steffen BE., Ölveczky, Bence P., 2018. The promise and perils of causal circuit manipulations. Curr. Opin. Neurobiol. 49, 84–94.

Wong, Kong-Fatt, Wang, Xiao-Jing, 2006. A recurrent network mechanism of time integration in perceptual decisions. J. Neurosci. 26 (4), 1314–1328.